


Chemical structure and optical signatures of
nitrogen acceptors in MgZnO†

Cite this: DOI: 10.1039/d0tc00826e

M. Zakria,^a P. Bove,^b D. J. Rogers,^{*b} F. H. Teherani,^b E. V. Sandana,^b M. R. Phillips^a
and C. Ton-That  ^{*,a}

The chemical and optical properties of wurtzite N-doped MgZnO epilayers with 16 at% Mg were grown by pulsed laser deposition and investigated using Near Edge X-ray Absorption Fine Structure (NEXAFS) and photoluminescence (PL) spectroscopy. When grown under nitrogen ambient the epilayers were an order of magnitude more resistive and displayed significantly different optical signatures compared with epilayers grown using similar conditions under oxygen or vacuum atmospheres. NEXAFS reveals that nitrogen in MgZnO:N exists in multiple chemical states with molecular N₂ and substitutional N on O sites (N_O) being the dominant species. The MgZnO:N epilayer exhibited a distinct PL peak centered at 3.45 eV, which possessed an activation energy of 48 meV and showed a blue shift with increasing excitation power density. This PL emission in the MgZnO:N epilayer was attributed to a shallow donor – deep acceptor pair recombination mechanism, where the compensating deep acceptor was most likely molecular N₂ at a Zn site. The results of this study offer the possibility of enhancing acceptor incorporation in oxides as well as for tuning their electrical and optical properties.

Received 18th February 2020,
Accepted 4th April 2020

DOI: 10.1039/d0tc00826e

rsc.li/materials-c

1. Introduction

Wide bandgap oxide-based semiconductors have emerged in recent years as important materials for use in a number of electronics and photonics applications.^{1,2} In spite of the lack of availability of reliable majority p-type doping, ZnO has become one of the most prevalent oxide semiconductors, thanks to a distinctive property set including a direct wide bandgap, intrinsically high transparency over the whole visible range, a high piezoelectric response and a resistivity that can be tuned from semi-insulating right through to semi-metallic by doping. Moreover, the bandgap of ZnO can be engineered upwards by alloying with MgO in order to fabricate UV sensors, solar cells, quantum wells and two-dimensional electron gases (2DEG) at MgZnO/ZnO heterointerfaces.^{3–5} Furthermore, it has been shown that epitaxial growth can allow MgZnO to retain the wurtzite structure up to 35 at% Mg,⁶ which takes this material into the class of ultrawide bandgap semiconductors and makes it potentially attractive for use in future high-power electronics.

Analogous to ZnO, the group VA elements N, P and Sb have been investigated as potential acceptor dopants in MgZnO.^{7–10}

Computational studies, supported by Raman measurements, indicate that alloying ZnO with MgO enhances the solubility of nitrogen by lowering the formation energy of substitutional N_O acceptors, and thereby increases the doping concentration.¹¹ Moreover, it has been shown that hole generation could be increased through the substitution of Zn by isovalent Mg, which shifts the conduction band minimum upwards and hence increases the ionization energies of compensating donors.^{12–14} Indeed, several groups have adopted MgZnO:N for the p-side in fabricating exploratory MgZnO bipolar homo-junction devices.^{8,15} However, considerable controversy still exists over the chemical identity of nitrogen acceptors in MgZnO. To date, most of the literature on N doping in MgZnO primarily relates to electrical characterization; however, much less is known about the nature of N acceptors themselves. Although UV emission bands in MgZnO close to the bandgap have been unambiguously assigned to neutral (D⁰X) and ionized donor bound excitons (D⁺X),^{16,17} neutral acceptor bound excitons (A⁰X) reported in the literature^{17,18} have not yet been unequivocally identified. Like ZnO, the benefits of MgZnO in broad device applications can only be realized once the optical and electrical activities of dopants and defects in this multifunctional material are established.

The aim of this work, therefore, was to obtain a detailed understanding of the chemical and optical properties of N acceptors in MgZnO:N. Although ion implantation would have been a viable technique to explore high nitrogen doping levels, this method generally creates significant damage to the crystal

^a School of Mathematical and Physical Sciences, University of Technology Sydney, Ultimo, New South Wales 2007, Australia. E-mail: cuong.ton-that@uts.edu.au

^b Nanovation, 8 Route de Chevreuse, 78117 Châteaufort, France.

E-mail: d.j.rogers@nanovation.com

† Electronic supplementary information (ESI) available. See DOI: 10.1039/d0tc00826e

lattice so an *in situ* approach was adopted in this study involving pulsed laser deposition (PLD). MgZnO epilayers were fabricated by PLD using identical conditions but under three different growth atmospheres (nitrogen, oxygen and vacuum). The chemical and optical properties of the MgZnO epilayers were then systematically investigated by Near Edge X-ray Absorption Fine Structure (NEXAFS) and photoluminescence (PL) spectroscopy. The results are in good agreement with the classical picture of nitrogen in ZnO, albeit with a significantly deeper acceptor level in MgZnO. This study establishes that nitrogen is primarily incorporated in MgZnO in the $(\text{N}_2)_{\text{Zn}}$ chemical state, which produces a strong signature donor-acceptor-pair (DAP) emission centered at 3.45 eV at 80 K. This, along with a marked increase in resistivity, indicates that $(\text{N}_2)_{\text{Zn}}$ is playing the role of a compensating deep acceptor in MgZnO.

2. Experimental section

ZnO layers were grown on *c*-sapphire substrates by PLD with a Coherent LPX 100 KrF (248 nm) excimer laser and a sintered ZnO target, as described elsewhere.¹⁹ MgZnO layers were then grown on the ZnO/*c*-sapphire layers using a high-purity 5 N MgZnO target with a composition of 4 wt% Mg in three different atmospheres (nitrogen, oxygen and vacuum) as previously described.²⁰ Low growth temperatures of $\sim 500^\circ\text{C}$ were adopted in order to overcome the low solubility of nitrogen in MgZnO. In this way, the incorporated nitrogen concentration was large enough to facilitate chemical analysis. The ZnO underlayer was 145 nm thick, while the thickness of the MgZnO layer was in the range of 215–330 nm as determined by optical reflection interferometry. Surface morphology was examined with a Park XE7 Atomic Force Microscopy (AFM) in non-contact mode. The crystal structure was studied using X-Ray Diffraction (XRD) in a high resolution Panalytical MRD Pro system using Cu $\text{K}\alpha_1$ radiation. Electrical resistivity was measured at several areas on each epilayer using a Signatone co-linear four-point probe system equipped with a Keithley 2400 source-meter. Hall measurements were not pursued because of the potential ambiguity related to samples being constituted of two conductive layers with significantly different electrical characteristics. Optical absorption was measured using a PerkinElmer Lambda 950 UV/VIS/NIR spectrometer. Correlative morphological and photoluminescence (PL) analysis of the samples was conducted in an FEI Quanta 200 Environmental SEM equipped with a Hamamatsu S7011-1007 CCD spectrometer. PL spectra were recorded using a He–Cd laser as an excitation source; the laser power density could be varied using a set of neutral density filters. The energy of laser photons (3.82 eV) was near and above the bandgap of MgZnO, allowing for an enhancement of the MgZnO luminescence emission relative to that from the ZnO underlayer. NEXAFS, implemented in the Total Fluorescence Yield (TFY) mode, was performed on the Soft X-ray Spectroscopy beamline at the Australian Synchrotron. The incident X-ray beam was perpendicular to the film surface. The photon

Table 1 Summary of *c* lattice parameter obtained from the XRD analysis of the ZnO underlayer and MgZnO/ZnO bilayers, FWHM of the rocking curve about (0002) reflection, RMS surface roughness for a $5 \times 5 \mu\text{m}^2$ AFM scan area, and electrical resistivity (ρ) at 300 K

Layer	<i>c</i> (Å)	Rock curve FWHM (°)	Roughness (nm)	ρ ($\Omega\text{ cm}$)
ZnO	5.218 ± 0.005	0.006	0.9	0.07
MgZnO:N/ ZnO	5.209 ± 0.05	0.095	5.3	0.60
MgZnO:O/ ZnO	5.162 ± 0.05	0.09	6.0	0.08
MgZnO:vac/ ZnO	5.223 ± 0.05	0.10	5.8	0.08

energy scale was calibrated against the Au $4f_{7/2}$ peak at 84 eV from a clean gold film in electrical contact with the sample.

3. Results and discussion

Table 1 shows a summary of the XRD, AFM and electrical resistivity findings. The XRD analysis reveals a wurtzite structure with strong preferential *c*-axis orientation along the growth direction for all the MgZnO/ZnO layers. Detailed structural analysis for the layers were described in our previous publication.²⁰ The ZnO underlayer shows distinct Pendellösung fringes and a *c*-lattice parameter of $5.218 \pm 0.005 \text{ \AA}$ (compared with the equilibrium value of 5.206 \AA), suggesting that the ZnO layer is under compressive strain in the basal plane. The ZnO layer also shows a remarkably low (0002) rocking curve full width half maximum (FWHM) value of $0.006 \pm 0.002^\circ$ indicating that there is a narrow dispersion in the crystallographic orientation about the *c*-axis. All the MgZnO/ZnO bilayers have significantly broadened $2\theta/\Omega$ peaks compared to the ZnO layer due to the superposition of the peaks from the ZnO underlayer and the MgZnO overlayer. These relatively broad peaks make the precise value of the *c*-lattice parameter ambiguous at 5.209 ± 0.05 , 5.162 ± 0.05 and $5.223 \pm 0.05 \text{ \AA}$, respectively, for the MgZnO:N/ZnO, MgZnO:O/ZnO and MgZnO:vac/ZnO layers. These values are, nevertheless, consistent with an epitaxial growth of MgZnO on ZnO.²¹ The XRD (0002) rocking curve FWHMs for all the MgZnO/ZnO bilayers are within a window of $0.095 \pm 0.005^\circ$, indicating that the dispersion in the crystallographic orientation about the *c*-axis is similar for all the MgZnO overlayers. The RMS roughness values for the three MgZnO/ZnO layers are similar and in the range of 5.3–6.0 nm. The resistivity for the MgZnO:N/ZnO layer is almost an order of magnitude higher than those for the layers grown under O_2 or vacuum. The reduction in the *n*-type conductivity in the MgZnO:N layer is similar to ZnO doping with N or Li, in which native donor defects are compensated by the acceptor dopant,²² and demonstrates the successful fabrication of N-doped MgZnO using the *in situ* doping method.

Fig. 1(a) shows the Tauc plot for the MgZnO/ZnO bilayers. There are sharp absorption edges at 3.38 eV and $\sim 3.6 \text{ eV}$, corresponding to the optical bandgaps of the ZnO underlayer and the MgZnO overlayer, respectively. The Tauc plots reveal that the band gap of the MgZnO:N layer is essentially the same

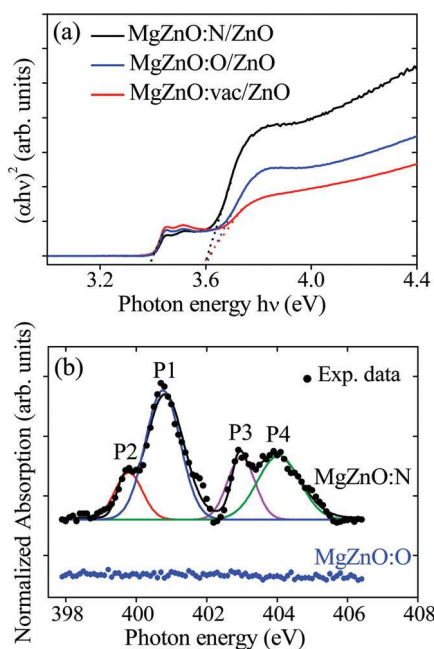


Fig. 1 (a) Tauc plots for optical absorption of the MgZnO/ZnO layers at 300 K, yielding a bandgap of 3.38 eV for the ZnO underlayer and ~ 3.6 eV for the MgZnO overlayer. (b) NEXAFS N K-edge spectra of MgZnO:O/ZnO and MgZnO:N/ZnO recorded in the bulk-sensitive TFY mode. The nitrogen content in the MgZnO:O/ZnO and MgZnO:vac/ZnO was below the NEXAFS detection limit. The spectrum of the MgZnO:N/ZnO is fitted with four mixed Gaussian–Lorentzian functions (the solid curve is the fit) corresponding to four different chemical states of nitrogen.

as that of MgZnO:O or MgZnO:vac within the experimental uncertainty. This result, combined with the XRD results, indicates that the nitrogen doping induces no changes in the band structure or crystalline quality of the MgO–ZnO alloy in this PLD fabrication route. A MgZnO bandgap of 3.6 eV corresponds to a Mg content of 16 at%.²³ To investigate the chemical states of nitrogen in MgZnO:N/ZnO, NEXAFS spectra were acquired around the N K-edge, which corresponds to resonant electron transitions from the N 1s initial state to the final unoccupied N-related state of *p*-symmetry. Fig. 1(b) shows the NEXAFS measurements for the MgZnO:N/ZnO and MgZnO:O/ZnO layers. The spectra for the MgZnO:O/ZnO and MgZnO:vac/ZnO (not shown) are featureless showing only background signal around the N K-edge since their nitrogen concentration is below the NEXAFS detection limit, which is about 1000 ppm (corresponding to 0.1%) under the experimental conditions used. However, the nitrogen concentration in the MgZnO:N layer was too low for the chemical analysis by photoelectron spectroscopy. The detection of nitrogen in the MgZnO:N layer is consistent with the observed $8\times$ increase in the film resistivity, compared with the layers grown under oxygen or vacuum ambient, due to donor compensation by nitrogen acceptors. The NEXAFS spectrum for the MgZnO:N/ZnO comprises four distinct resonant peaks (labelled P1 to P4). The strong resonance P1 at 400.7 eV is consistent with the characteristic N 1s to π^* transition in N–N species.²⁴ To the best of our knowledge, there are no NEXAFS data for nitrogen in

MgZnO; however, a similar sharp resonance peak, close to the P1 position, has previously been ascribed to molecular nitrogen in ZnO,²⁵ GaN,²⁶ and InN²⁷ that were doped with N ions. Accordingly, we attribute the resonance P1 to nitrogen molecules in MgZnO:N. The shoulder P2, at 399.7 eV, is at the same position as the resonance previously observed in N-doped ZnO crystals and can be assigned to the transition involving N $2p\pi^*$ and Zn 3d hybridised orbitals.^{25,28} The structural resemblance of P2 in MgZnO and ZnO indicates the formation of N–Mg and N–Zn bonds, consistent with nitrogen substitution on oxygen sites (N_O) in the lattice. The higher energy components, P3 and P4, are close to the characteristic absorption peaks of various nitrogen oxides, such as NO₂ (at 403.2 eV) and N₂O (at 404.5 eV),^{28,29} which indicates the existence of substitutional N on Zn sites in the MgZnO:N epilayer. It is proposed, therefore, that nitrogen ions are present in several oxidation states in MgZnO, in addition to the configurations N_O and N_Z , by forming N–O, O–N–O and N–N–O bonds. The relative intensities of the nitrogen chemical states were obtained by deconvoluting the N K-edge spectrum using a Gaussian–Lorentzian function, as shown in Fig. 1(e), showing that about half of nitrogen exists in the N_Z state while only $\sim 13\%$ is in the N_O states.

The PL spectra for the MgZnO:N/ZnO, MgZnO:O/ZnO and MgZnO:vac/ZnO bilayers and the ZnO underlayer are displayed in Fig. 2(a). Two sharp peaks at 3.352 and 3.373 eV, observed in all PL spectra, are attributed to the radiative recombination of free excitons (FX) and donor-bound excitons (DX) in the ZnO underlayer, respectively.³⁰ Additionally, all epilayers exhibit a periodic set of peaks at 3.519, 3.592, 3.665 and 3.739 eV as a result of multiphonon resonant Raman scattering (RRS).³¹ These sharp Raman peaks are separated from the HeCd 3.812 eV laser line by multiples of the longitudinal optical phonon energy of MgZnO, $E_{LO} = 73$ meV, where the Raman peak position (E_{RRS}^n) is given by $E_{RRS}^n = 3.812 - nE_{LO}$ eV ($n = 1, 2, 3, 4$).³² Significantly, the MgZnO:O and MgZnO:vac epilayers exhibit a near-band-edge (NBE) band peaked at 3.61 eV, which is consistent with the band gap measured using the Tauc plot in Fig. 1(c). The presence of the RRS peaks and the relatively weak NBE emission from the MgZnO layers, compared with the ZnO underlayer, are consistent with the effect of potential fluctuations in the MgZnO alloy.^{31,32} The broadening of the MgZnO NBE peak is most likely caused by lattice disorder arising from the high Mg content. In comparison, the MgZnO:N/ZnO bilayer shows an additional broad PL emission centered at 3.45 eV, which is 160 meV below the MgZnO NBE. This rules out its assignment to a N acceptor bound exciton emission that is reported to be to less than 100 meV below the bandgap of MgZnO films.^{18,33} The 3.45 eV PL emission in the MgZnO:N is similar to a previously reported shallow donor-to-acceptor (DAP) transition in N-doped ZnO at 120 meV below the NBE.^{22,25} This result indicates that the nitrogen acceptor level in MgZnO:N is ~ 40 meV deeper than in ZnO:N, assuming that the binding energy of the dominant donor in ZnO and MgZnO is similar. This deeper nature of N acceptors in MgZnO:N is in agreement with the expected downward shift (ΔE_{VB}) of the $Mg_{0.16}Zn_{0.84}O$ valence band maximum relative to the ZnO level

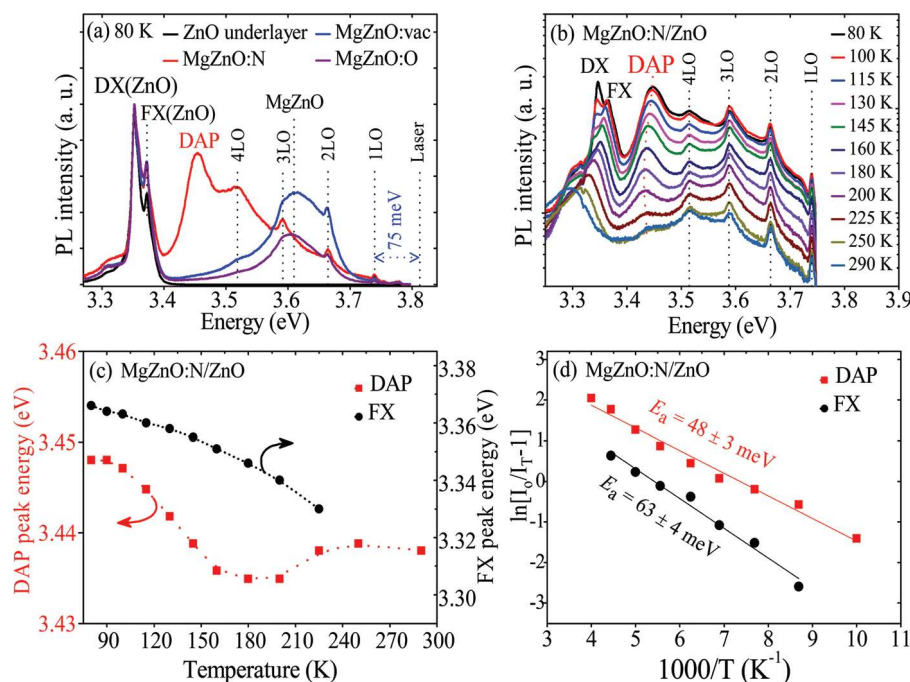


Fig. 2 (a) PL spectra for the MgZnO/ZnO bilayers and ZnO underlayer ($T = 80$ K, $E_{\text{laser}} = 3.814$ eV). The MgZnO:N/ZnO exhibits a pronounced DAP emission at 3.45 eV due to nitrogen acceptors. The FX and DX emission peaks originate from the ZnO underlayer. The four sharp Raman peaks (labelled 1LO, 2LO, 3LO and 4LO) are separated from the laser line by multiples of the LO phonon energy, $E_{\text{LO}}(\text{MgZnO}) = 73$ meV. (b) Temperature-resolved PL spectra for the MgZnO:N/ZnO with a logarithmic intensity scale. (c) Peak energies for the ZnO FX and MgZnO N-related DAP emissions in MgZnO:N/ZnO as a function of temperature. The FX peak red shifts monotonically with increasing temperature, while the DAP follows an “S-shape” emission shift due to compositional fluctuations. (d) Arrhenius plots yielding $E_a = 48 \pm 3$ eV and $E_a = 63 \pm 4$ eV for the MgZnO DAP and ZnO FX, respectively.

due to the ZnO/MgZnO band offsets; as in, for example, Ohtomo *et al.*,³⁴ which reports a $\Delta E_{\text{VB}} = 46$ meV for ZnO/Mg_{0.2}Zn_{0.8}O. The DAP emission shift from the NBE emission is also comparable with the reported level of $E_v + 160$ meV measured by deep level optical spectroscopy for acceptors in N-doped MgZnO with 10 at% Mg.¹⁴

Temperature dependence of the radiative transitions gives insights into the thermal behaviour and activation energies of the recombination channels. Fig. 2(b) displays the temperature-resolved PL spectra for the ZnO NBE and MgZnO:N emission bands. (For the temperature-resolved PL spectra of the undoped MgZnO layers, see ESI† Fig. S1.) With increasing temperature, the ZnO DX emission is quenched rapidly as neutral shallow donors become increasingly unavailable for radiative recombination as a result of their thermal ionization. Concurrently, the intensity of the ZnO FX peaks decreases, broadens and red shifts due to the effects of lattice dilation and electron–phonon interaction at low and elevated temperatures, respectively. In a similar manner, the MgZnO NBE, at around 3.6 eV, shifts to lower energy and quenches with increasing temperature, whereas the intensity of the MgZnO N-related DAP is rather independent of temperature up to 130 K. As expected, being independent of temperature, the positions of the sharp RRS emission peaks remain constant as marked by vertical dotted lines. Fig. 2(c) shows the temperature dependence of the peak position of the MgZnO:N DAP peak and the ZnO FX for comparison. The plot reveals that the DAP initially red shifts

from 80 to 180 K and then blue shifts from 180 K. This “S-shape” profile is highly characteristic of DAP recombination in semiconductor alloys with significant band edge potential variations caused by compositional fluctuations.³⁵ Here, as the temperature increases from 80 K, photogenerated carriers are able to populate from deeper local potential minima arising from compositional fluctuations, which produces the observed red shift. With a further temperature rise above 180 K, these deep states empty due to thermal ionization, leading to the blue shift in the peak position. The DAP blue shift could result from shallow donor thermal ionization. However, Fig. 2(c) shows that the DAP red shifts at a much slower rate than the FX with increasing temperature, which supports the thermal fluctuation mechanism. Since the 3.45 eV peak is completely absent in the MgZnO:O/ZnO and MgZnO:vac/ZnO bilayers, this “S-shape” behavior strongly supports the assignment of the 3.45 eV PL emission in the MgZnO:N/ZnO bilayer to DAP recombination involving a N deep acceptor. The Arrhenius plots of the ZnO FX and MgZnO:N DAP intensities are shown in Fig. 2(d), yielding activation energies of 63 ± 4 and 48 ± 3 meV, respectively. The measured E_a value for the FX is consistent with the exciton binding energy of ZnO (60 meV) and associated with thermal disassociation of excitons. The 48 meV E_a value of the MgZnO:N DAP is similar to the reported binding energies (43 and 56 meV) for nitrogen acceptors in MgZnO films,¹⁸ however, this E_a value is too low to be logically ascribed to thermal ionization of the nitrogen acceptor involved in the 3.45

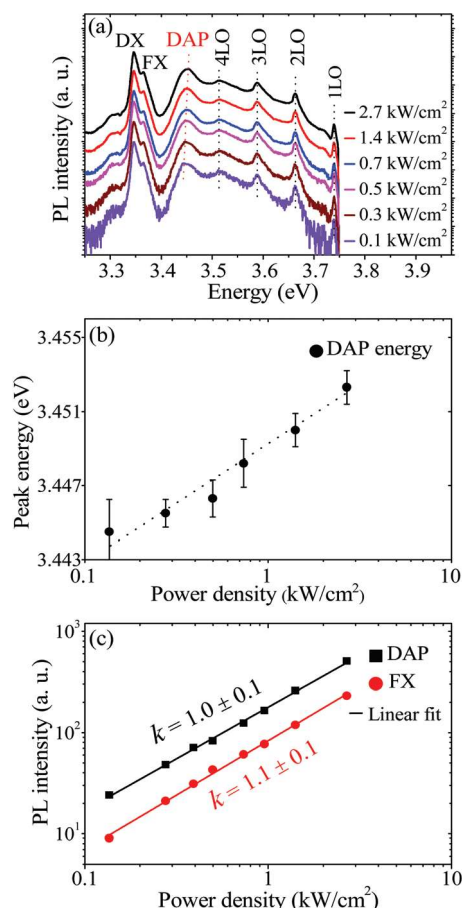


Fig. 3 (a) Power-resolved PL spectra of the MgZnO:N/ZnO bilayer at 80 K for excitation power densities ranging from 0.1 to 2.7 kW cm⁻². The MgZnO:N DAP peak gradually blue shifts with increasing excitation density, while the FX(ZnO), DX(ZnO) and RRS peak positions remain unchanged. (b) Blue shift of the DAP peak by ~8 meV over the measured power density range, characteristic of a DAP emission. (c) Log-log plot of the ZnO FX and MgZnO DAP integrated intensities as a function of excitation density. The lines are the fits to the power-law model $I_{PL} \propto I_{laser}^k$ with a power exponent $k = 1.0$ and 1.1 for the DAP and FX emissions, respectively.

eV emission, which has much greater binding energy as estimated above. Accordingly, the 48 meV activation energy of the MgZnO DAP is assigned to the binding energy of the dominant donor in the MgZnO layers.

To confirm the nature of the emission bands, we conducted power-dependent PL measurements for the MgZnO:N/ZnO bilayer (Fig. 3). With increasing laser intensity, the FX and RRS peak positions remain unchanged, whereas the 3.45 eV band gradually shifts to higher energies as shown in Fig. 3(b). This blueshift with increasing excitation power is characteristic of DAP transitions and is explained by the Coulombic interaction between spatially separated donor-acceptor pairs at different distances.²² The emission energy of the DAP is given by the following relationship,

$$h\nu(\text{DAP}) = E_g - (E_A + E_D) + \frac{e^2}{4\pi\epsilon r} \quad (1)$$

where E_g is the bandgap, r is the distance between donor-

acceptor pairs, E_A and E_D are the donor and acceptor binding energies, respectively. The last term accounts for the Coulombic interaction between the ionized donor and ionized acceptor pairs involved in the radiative DAP recombination transition. For the overlap between the wave functions of the donor and acceptor to be significant, r is typically less than ~2.5 nm.³⁶ Using this value and $E_D = 48$ meV, eqn (1) results in $E_A \approx 169$ meV, which confirms that the nitrogen acceptor level in MgZnO:N is deeper than in ZnO:N, as estimated above. With increasing the excitation power density from 0.1 to 3 kW cm⁻² (see Fig. 3b), the DAP blue shifts about ~8 meV, which originates from the saturation of distant pairs with long lifetimes and a redistribution of the DAP recombination to closer pairs with a larger Coulombic interaction. The power density excitation data are further analyzed using the power-law model $I_{PL} \propto I_{laser}^k$, where I_{PL} is the integrated PL intensity and I_{laser} is the laser intensity. The log-log plots based on the power-law model are displayed in Fig. 3(c), which yields a power-law exponent $k \approx 1$ within the experimental error of the measurement for both the ZnO FX and MgZnO DAP bands. The linear dependence of the FX on excitation density is expected because of the fast excitonic recombination lifetimes, typically <1 ns.³⁷ However, with DAP recombination a sub-linear power-law exponent is generally expected due to saturation of the deep-level defect involved in the radiative transition. The linear DAP intensity dependence on excitation density observed for the MgZnO:N indicates that the deep level is not saturated under our excitation regime, which suggests the presence of a relatively high concentration of N acceptors.

Our NEXAFS studies reported above reveal the existence of several chemical states of N-related defects that are possible candidates for the deep acceptor in the 3.45 eV DAP transition observed in the MgZnO:N sample. Nitrogen is an amphoteric impurity in ZnO and can act, therefore, as either a donor or an acceptor impurity. Indeed, our NEXAFS results shown in Fig. 1(b) reveal the incorporation of both types of dopants in MgZnO:N. Here, the P1 and P2 peaks are attributed to the presence of N₂ molecules and N_O acceptor states, respectively, while the P3 and P4 resonances were assigned to substitutional N on Zn sites, which act as donors. The significant concentration of these donor centers in the MgZnO:N sample is probably due to non-equilibrium PLD growth conditions at relatively low temperatures. In ZnO, isolated N_O is a deep acceptor, with the (0/-) level 1.3 eV above the valence band maximum,³⁸ thus this state is clearly too deep to act as an acceptor in the 3.45 eV DAP emission. It has been proposed that the N_O-V_{Zn} complex could produce a shallower defect level at 160 meV; however, such a complex would be thermodynamically unfavorable in low-temperature PLD growth as there is a huge potential barrier of 1.1 eV to its formation.³⁹ (N₂)_O is a shallow donor, which cannot explain the acceptor involved in the observed DAP emission. In contrast, when occupying a cation site, (N₂)_{Zn} has been predicted to be a shallow double acceptor with a binding energy of ~120 meV,⁴⁰ and would be deeper by ~22 meV in Mg_{0.16}Zn_{0.84}O due to the downward shift of the MgZnO valence band edge relative to that of ZnO.³⁴

These results, coupled with our observation that N_2 is the dominant state in the $MgZnO:N$, make the $(N_2)_{Zn}$ state the most likely candidate for the acceptor in the 3.45 eV DAP emission. Given the fact that NEXAFS is highly sensitive to the local bonding environment of nitrogen in the lattice, the similarity of the P1 peak energy in the $MgZnO:N$ NEXAFS spectrum to other molecular N_2 peaks previously recorded in nitrides and oxides (such as GaN , InN and ZnO)²⁶ suggests that N_2 molecules in $MgZnO:N$ are only weakly bound to the lattice.

4. Conclusions

$MgZnO$ epilayers (with 16 at% Mg) grown by PLD in a nitrogen ambient facilitates nitrogen doping to a level where its chemical states could be identified by NEXAFS. Such a large dopant concentration was achieved by growing epitaxial $MgZnO$ on a ZnO underlayer using low-temperature growth which favours the incorporation of nitrogen. Four point electrical measurements showed a significantly increased resistivity for the $MgZnO:N$ epilayer compared with the $MgZnO:O$ and $MgZnO:vac$ epilayers grown under similar conditions. PL spectroscopy revealed a N-related 3.45 eV DAP band that was absent in $MgZnO:O$ and $MgZnO:vac$ epilayers, which exhibited comparable band-edge emission at 3.6 eV. The DAP band in $MgZnO:N$ is located at 160 meV below the band-edge emission and has an activation energy of 48 meV. It was found that nitrogen dopants existed mostly in the molecular state, which weakly bonds to the $MgZnO$ lattice. Based on the experimental evidence, it is suggested that (i) the DAP emission in $MgZnO:N$ is due to radiative recombination involving deep $(N_2)_{Zn}$ acceptors and shallow donors and (ii) the high concentration of $(N_2)_{Zn}$ acceptors act to effectively compensate the predominant n-type conductivity and thus renders the $MgZnO:N$ layers significantly more resistive.

Conflicts of interest

There are no conflicts to declare.

Acknowledgements

This research is supported by the Global Connections Fund (Bridging grant 279322689) of the Australian Academy of Technology and Engineering and Australian Research Council (ARC) Discovery Project funding scheme (project number DP150103317). The work was partly undertaken on the Soft X-ray Spectroscopy beamline at the Australian Synchrotron, Victoria, Australia. We also acknowledge the technical assistance of Anton Tadich, Bruce Cowie, Mark Lockrey and Olivier Lee.

References

- M. Lorenz, M. S. R. Rao, T. Venkatesan, E. Fortunato, P. Barquinha, R. Branquinho, D. Salgueiro, R. Martins, E. Carlos, A. Liu, F. K. Shan, M. Grundmann, H. Boschker, J. Mukherjee, M. Priyadarshini, N. DasGupta, D. J. Rogers, F. H. Teherani, E. V. Sandana, P. Bove, K. Rietwyk, A. Zaban, A. Veziridis, A. Weidenkaff, M. Muralidhar, M. Murakami, S. Abel, J. Fompeyrine, J. Zuniga-Perez, R. Ramesh, N. A. Spaldin, S. Ostanin, V. Borisov, I. Mertig, V. Lazenka, G. Srinivasan, W. Prellier, M. Uchida, M. Kawasaki, R. Pentcheva, P. Gegenwart, F. M. Granozio, J. Fontcuberta and N. Pryds, *J. Phys. D: Appl. Phys.*, 2016, **49**, 433001.
- H. Y. Hwang, Y. Iwasa, M. Kawasaki, B. Keimer, N. Nagaosa and Y. Tokura, *Nat. Mater.*, 2012, **11**, 103–113.
- A. Tsukazaki, A. Ohtomo, T. Kita, Y. Ohno, H. Ohno and M. Kawasaki, *Science*, 2007, **315**, 1388–1391.
- X. L. Zhang, K. Welch, L. Tian, M. B. Johansson, L. Haggman, J. H. Liu and E. M. J. Johansson, *J. Mater. Chem. C*, 2017, **5**, 11111–11120.
- I. A. Solov'ev, S. V. Poltavtsev, Y. V. Kapitonov, I. A. Akimov, S. Sadofev, J. Puls, D. R. Yakovlev and M. Bayer, *Phys. Rev. B*, 2018, **97**, 245406.
- I. Takeuchi, W. Yang, K.-S. Chang, M. Aronova, T. Venkatesan, R. Vispute and L. Bendersky, *J. Appl. Phys.*, 2003, **94**, 7336–7340.
- R. C. Wang, Y. X. Lin and J. J. Wu, *J. Phys. Chem. C*, 2015, **119**, 29186–29192.
- Y. W. Heo, Y. W. Kwon, Y. Li, S. J. Pearton and D. P. Norton, *Appl. Phys. Lett.*, 2004, **84**, 3474–3476.
- Z. Wei, B. Yao, Z. Zhang, Y. Lu, D. Shen, B. Li, X. Wang, J. Zhang, D. Zhao and X. Fan, *Appl. Phys. Lett.*, 2006, **89**, 102104.
- B. H. Kim, M. W. Kim, J. W. Kang, Y. S. Choi, B. J. Kim and S. J. Park, *J. Alloys Compd.*, 2018, **757**, 98–104.
- Y. Gai, B. Yao, Z. Wei, Y. Li, Y. Lu, D. Shen, J. Zhang, D. Zhao, X. Fan and J. Li, *Appl. Phys. Lett.*, 2008, **92**, 062110.
- J. Li, S.-H. Wei, S.-S. Li and J.-B. Xia, *Phys. Rev. B: Condens. Matter Mater. Phys.*, 2006, **74**, 081201.
- L. L. Gao, B. Yao, B. Liu, L. Liu, T. Yang, B. B. Liu and D. Z. Shen, *J. Chem. Phys.*, 2010, **133**, 204501.
- A. Kurtz, A. Hierro, E. Munoz, S. K. Mohanta and A. Nakamura, *Appl. Phys. Lett.*, 2014, **104**, 081105.
- C. X. Shan, J. S. Liu, Y. J. Lu, B. H. Li, F. C. C. Ling and D. Z. Shen, *Opt. Lett.*, 2015, **40**, 3041–3044.
- M. Trunk, V. Venkatachalapathy, A. Galeckas and A. Y. Kuznetsov, *Appl. Phys. Lett.*, 2010, **97**, 211901.
- Y. F. Li, B. Yao, Y. M. Lu, Z. P. Wei, Y. Q. Gai, C. J. Zheng, Z. Z. Zhang, B. H. Li, D. Z. Shen, X. W. Fan and Z. K. Tang, *Appl. Phys. Lett.*, 2007, **91**, 232115.
- Z. Wei, B. Yao, X. Wang, Z. Zhang, Y. Lu, D. Shen, B. Li, J. Zhang, D. Zhao and X. Fan, *J. Mater. Res.*, 2007, **22**, 2791–2795.
- D. J. Rogers, D. C. Look, F. H. Teherani, K. Minder, M. Razeghi, A. Largeau, G. Demazeau, J. Morrod, K. A. Prior, A. Lusson and S. Hassani, *Phys. Status Solidi C*, 2008, **5**, 3084.
- D. J. Rogers, F. H. Teherani, P. Bove, A. Lusson and M. Razeghi, *Oxide-Based Materials and Devices IV*, Proc. SPIE 8626, 86261X, San Francisco, 2013.

- 1 21 Y. Nishimoto, K. Nakahara, D. Takamizu, A. Sasaki, K. Tamura, S. Akasaka, H. Yuji, T. Fujii, T. Tanabe, H. Takasu, A. Tsukazaki, A. Ohtomo, T. Onuma, S. F. Chichibu and M. Kawasaki, *Appl. Phys. Express*, 2008, **1**, 091202. 1
- 5 22 S. Lautenschlaeger, S. Eisermann, G. Haas, E. A. Zolnowski, M. N. Hofmann, A. Laufer, M. Pinnisch, B. K. Meyer, M. R. Wagner and J. S. Reparaz, *Phys. Rev. B: Condens. Matter Mater. Phys.*, 2012, **85**, 235204. 5
- 10 23 J. Liu, C. Shan, S. Wang, B. Li, Z. Zhang and D. Shen, *J. Cryst. Growth*, 2012, **347**, 95–98. 10
- 24 G. R. Wight and C. E. Brion, *J. Electron Spectrosc. Relat. Phenom.*, 1974, **4**, 313–325.
- 15 25 C. Ton-That, L. Zhu, M. Lockrey, M. Phillips, B. Cowie, A. Tadich, L. Thomsen, S. Khachadorian, S. Schlichting and N. Jankowski, *Phys. Rev. B: Condens. Matter Mater. Phys.*, 2015, **92**, 024103. 15
- 26 B. J. Ruck, A. Koo, U. D. Lanke, F. Budde, S. Granville, H. J. Trodahl, A. Bittar, J. B. Metson, V. J. Kennedy and A. Markwitz, *Phys. Rev. B: Condens. Matter Mater. Phys.*, 2004, **70**, 235202. 20
- 27 A. Bozanic, Z. Majlinger, M. Petravic, Q. Gao, D. Llewellyn, C. Crotti and Y. W. Yang, *J. Vac. Sci. Technol., A*, 2008, **26**, 592–596.
- 25 28 C. Zou, X. Yan, J. Han, R. Chen, W. Gao and J. Metson, *Appl. Phys. Lett.*, 2009, **94**, 171903. 25
- 29 J. G. Chen, *Surf. Sci. Rep.*, 1997, **30**, 1–152.
- 30 M. R. Wagner, G. Callsen, J. S. Reparaz, J. H. Schulze, R. Kirste, M. Cobet, I. A. Ostapenko, S. Rodt, C. Nenstiel, M. Kaiser, A. Hoffmann, A. V. Rodina, M. R. Phillips, S. Lautenschlager, S. Eisermann and B. K. Meyer, *Phys. Rev. B: Condens. Matter Mater. Phys.*, 2011, **84**, 035313. 5
- 31 V. Ursaki, I. Tiginyanu, V. Zalamai, E. Rusu, G. Emelchenko, V. Masalov and E. Samarov, *Phys. Rev. B: Condens. Matter Mater. Phys.*, 2004, **70**, 155204.
- 32 J. Ye, K. Teoh, X. Sun, G. Lo, D. Kwong, H. Zhao, S. Gu, R. Zhang, Y. Zheng and S. Oh, *Appl. Phys. Lett.*, 2007, **91**, 091901. 10
- 33 S. Saha, S. K. Pandey, S. Nagar and S. Chakrabarti, *J. Mater. Sci.: Mater. Electron.*, 2015, **26**, 9759–9765.
- 34 A. Ohtomo, M. Kawasaki, I. Ohkubo, H. Koinuma, T. Yasuda and Y. Segawa, *Appl. Phys. Lett.*, 1999, **75**, 980–982.
- 35 B. Han, M. P. Ulmer and B. W. Wessels, *Phys. B*, 2003, **340**, 470–474. 15
- 36 M. A. Reshchikov and H. Morkoc, *J. Appl. Phys.*, 2005, **97**, 061301.
- 37 C. Ton-That, L. Weston and M. R. Phillips, *Phys. Rev. B: Condens. Matter Mater. Phys.*, 2012, **86**, 115205. 20
- 38 J. L. Lyons, A. Janotti and C. G. Van de Walle, *Appl. Phys. Lett.*, 2009, **95**, 252105.
- 39 L. Liu, J. L. Xu, D. D. Wang, M. M. Jiang, S. P. Wang, B. H. Li, Z. Z. Zhang, D. X. Zhao, C. X. Shan, B. Yao and D. Z. Shen, *Phys. Rev. Lett.*, 2012, **108**, 215501. 25
- 40 W. R. L. Lambrecht and A. Boonchun, *Phys. Rev. B: Condens. Matter Mater. Phys.*, 2013, **87**, 195207.

30

30

35

35

40

40

45

45

50

50

55

55